Shock Waves
DOI 10.1007/s00193-011-0332-0

ORIGINAL ARTICLE

Growth rate predictions of single- and multi-mode Richtmyer–Meshkov instability with reshock

S. Ukai · K. Balakrishnan · S. Menon

Received: 7 June 2010 / Revised: 24 February 2011 / Accepted: 18 May 2011

Abstract The single- and multi-mode Richtmyer–Meshkov instabilities (RMI) with reshock are numerically analyzed in two- and three-dimensional domains. Four different types of air/SF_6 interface shapes are investigated in a shock tube configuration, and the predicted post-reshock growth rates are compared with available empirical models of Mikaelian's (Physica D 36(3):343–347, 1989) and Charakhch'an's (J Appl Mech Tech Phys 41(1):23–31, 2000). The simulation of 3D multi-mode RMI shows good agreement with a past experimental study, but other interface types (2D single-mode, 2D multi-mode and 3D single-mode) result in different growth rates after reshock. Parametric studies are therefore performed to investigate the sensitivities of the post-reshock growth rates to model the empirical parameters. For single-mode RMI configurations, the interface shape is found to be only a weak function of the post-reshock growth rate, as also predicted by previous reshock models. The post-reshock growth rate shows a linear correlation to the velocity jump due to reshock; however, it is only about a half of the prediction of Charakhch'an's model even though the growth before reshock compares well with pre-reshock models. The 3D single-mode post-reshock RMI growth rate is nearly 1.6 times larger than the 2D single-mode RMI. The parametric studies of multi-mode RMI show two distinctly different growth rates depending on the mixing conditions at reshock. If the interface remains sharp at the time of reshock, the post-reshock growth rate is as large as the single-mode cases. However, if the interface is mixed due to non-linear interactions of bubbles and spikes, the growth rates becomes slow and independent of the interface shapes. Overall, this study provides new insights into the flow features of reshocked RMI for different initial perturbation types.

Keywords Richtmyer–Meshkov instability · Shock wave · Reshock · Perturbation · Mixing

Communicated by E. Timofeev.

S. Ukai · K. Balakrishnan · S. Menon (✉)
School of Aerospace Engineering, Georgia Institute of Technology, Atlanta, GA 30332-0150, USA
e-mail: suresh.menon@aerospace.gatech.edu

Present Address:
S. Ukai
Institut für Technische Verbrennung, Universität Stuttgart, 70174 Stuttgart, Germany

Present Address:
K. Balakrishnan
Computational Research Division, Lawrence Berkeley National Laboratory, Berkeley, CA 94720, USA

1 Introduction

Richtmyer–Meshkov instability (RMI) occurs when an interface between two media of different densities is impulsively accelerated, for instance by a shock wave. This phenomenon was first theoretically proven by Richtmyer [1], and later experimentally verified by Meshkov [2]. RMI occurs in various natural and engineering situations such as supernovae explosions [3], deflagration-to-detonation transition [4], confinement fusion [5], and fuel mixing in a scramjet [6]. The RMI evolution can be characterized by the inviscid compressible vorticity equation [7,8]:

$$\frac{\mathrm{D}\boldsymbol{\omega}}{\mathrm{D}t} = \underbrace{\frac{\nabla\rho\times\nabla p}{\rho^2}}_{\text{baroclinic production}} + \underbrace{\boldsymbol{\omega}\cdot\nabla\boldsymbol{u}}_{\text{vortex stretching}} - \underbrace{\boldsymbol{\omega}(\nabla\cdot\boldsymbol{u})}_{\text{vortex dilatation}}, \quad (1)$$

where p denotes the pressure, ρ is the density, $\boldsymbol{u}$ is the velocity, $\boldsymbol{\omega} = \nabla\times\boldsymbol{u}$ is the vorticity, and $\mathrm{D}/\mathrm{D}t = \partial/\partial t + \boldsymbol{u}\cdot\nabla$.

Published online: 24 August 2011

A driving mechanism of RMI is the baroclinic torque vorticity production term that is caused by a misalignment of the pressure and density gradients. When a shock interacts with the perturbed interface, vorticity is deposited by this baroclinic term, and the interface is subsequently accelerated based on the direction of vorticity. This interface perturbation can be considered as a combination of a bubble and a spike [9], where a bubble is the region where the lighter fluids penetrates into the heavier fluid, and a spike is the region where the heavier fluid penetrates into the lighter fluid (Fig. 1). To quantify RMI evolution, one can define the mixing length, h, as the distance between the spike and the bubble tips, a mean amplitude, $a = h/2$, and the amplitudes, a_b and a_s, as the distance from the unperturbed interface location to bubble or spike tip, respectively.

Unlike the Rayleigh–Taylor instability (RTI) [10], which is driven by a continuous acceleration, RMI is unstable in either a light-heavy or a heavy-light configuration (Fig. 2) [7]. A shock propagating from the light gas side (light–heavy configuration) deposits vorticity that can amplify the original perturbation. On the other hand, if the shock is approaching from the heavy gas side (heavy–light configuration), the vorticity causes interface motion initially to reduce the perturbation, and spikes and bubbles are eventually inverted and grow in opposite directions [7].

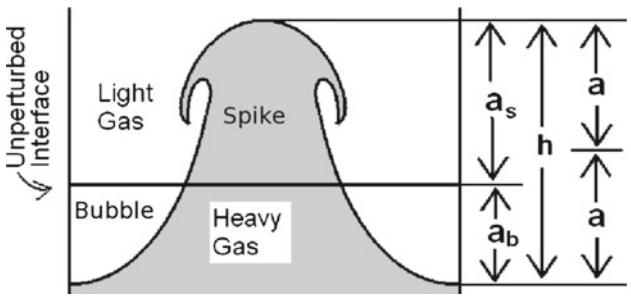

Fig. 1 Bubble and spike definition for a RMI perturbation. The *gray* and *white* regions correspond to the heavy and light species, respectively

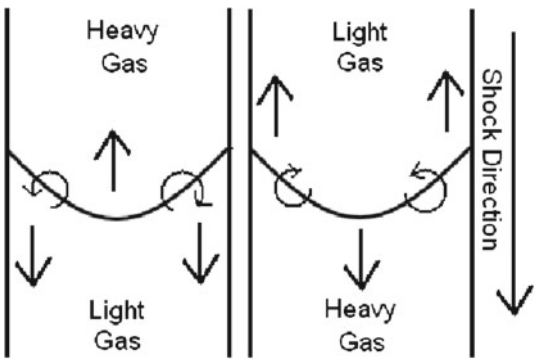

Fig. 2 Vorticity deposition over a species interface with heavy–light (*left*) and light–heavy (*right*) configurations

Growth rates of single-mode RMI have been studied for over fifty years. Richtmyer [1] originally developed a linear growth model of the amplitude, $a(t)$ based on an impulsive model:

$$a(t) = a_0 + v_0 t, \tag{2}$$

where a_0 is the initial amplitude, v_0 is the Richtmyer velocity defined as $v_0 = ka_0 A \Delta V_1$, k is the wavenumber given as $k = 2\pi/\lambda$, λ is the wavelength, A is the Atwood number defined as $A = (\rho_2 - \rho_1)/(\rho_2 + \rho_1)$, and ΔV_1 is the change in the speed of the interface due to an incident shock. Here, ρ_1 and ρ_2 denote, respectively, the densities of the light and heavy fluids. The impulsive model is only applicable in the linear-regime where $ka < 0.3$ [11]. Therefore, non-linear models have been developed to predict the late time growth rates. A potential flow model for RTI [12] was extended to RMI [13,14], but such models in the early days were limited to $A = 1$ (fluid-vacuum interface) and were only applicable to obtain the initial and the asymptotic (time $\rightarrow \infty$) growth rates [13–15]. To deal with the constraints of potential flow models, several Padé approximation based models have been developed [16–18] to numerically obtain the time-dependent solution with an arbitrary Atwood number. However, these approximation methods were not very successful [19] because even very high order approximations depart from the solution at late times. More recently, Goncharov [20] developed a potential flow model for an arbitrary Atwood number, and Mikaelian [21] extended Goncharov's work to obtain an explicit time-dependent expression. Sadot et al. [22] obtained an empirical expression to link the initial and asymptotic solution of the potential flow model [13]. The advantage of this empirical model is that the coefficients can be modified to adapt to different analytical models [19]. Past studies have employed 2D [11,19,23,24] and 3D [25,26] single-mode RMI experiments and numerical analysis to evaluate and identify the domain of applicability of these models.

Recently, the Richtmyer–Meshkov instability involving multiple shocks has been studied. The RMI with multiple shocks is seen in many confined systems, such as shock tubes [27–29] and blast waves [30,31], and it has been shown that the impulsive acceleration of the evolving interface demonstrates different growth behaviors. For example, RMI with a second shock (often termed as a reshock) has been shown to cause a rapid increase of growth rates and thereby enhance the amount of mixing [27–29].

Even though the growth models of single-mode RMI are well established, the post-reshock models are still in their infancy. The change in the growth rate due to reshock was first analytically studied by Mikaelian [32] by applying the potential flow model of the single-mode RMI to a growing perturbation; the criteria to determine whether the second shock accelerates, decelerates, freezes out, or inverts the

perturbation were analyzed. Extending the impulsive model (2), the growth rate after reshock can be written as:

$$\frac{\mathrm{d}h_2}{\mathrm{d}t} = \frac{2\pi h_\mathrm{r}}{\lambda}\Delta V_2 A - \frac{\mathrm{d}h_1}{\mathrm{d}t}. \tag{3}$$

Also, Brouillette and Sturtevant [33] developed a similar model for multiple shock systems. However, both these models are a function of the wavelength and mixing length at reshock, h_r, and they are only applicable when the mixing length at the second shock is very small ($h_\mathrm{r} \ll \lambda$) as originally assumed in Richtmyer's model (2). Due to the very complex interface shapes at reshock, it is difficult to construct analytic models, and so two empirical models applicable to specific interface configurations have been developed. Charakhch'an [34] formulated a model from the numerical studies of single-mode 2D RMI with reshock; it was found that the growth rate is only a weak function of h_r and k at the second shock. The following empirical expression was derived [34]:

$$\frac{\mathrm{d}h_2}{\mathrm{d}t} = \beta\Delta V_2 A - \frac{\mathrm{d}h_1}{\mathrm{d}t}, \tag{4}$$

where $\frac{\mathrm{d}h_1}{\mathrm{d}t}$ is the growth rate immediately before the reshock, and $\beta = 1.25$ from multiple numerical results. Note that $\frac{\mathrm{d}h_1}{\mathrm{d}t}$ and $\frac{\mathrm{d}h_2}{\mathrm{d}t}$ have opposite signs as they correspond to perturbation growths in opposite directions. Interestingly, if $\beta = \frac{2\pi h_\mathrm{r}}{\lambda}$, (4) follows (3). However, Charakhch'an claimed that the coefficient used in the above equation is constant and independent of h_r and λ.

The second type of model is Mikaelian's reshock model [35] developed for multi-mode 3D perturbation, and uses the following linear correlation:

$$\frac{\mathrm{d}h_2}{\mathrm{d}t} = C\Delta V_2 A^+, \tag{5}$$

where $\frac{\mathrm{d}h_2}{\mathrm{d}t}$ is the growth rate after reshock, ΔV_2 is the velocity jump caused by the second shock, A^+ is the post-reshock Atwood number, and $C = 0.28$ is an empirically determined constant from experimental RTI studies [36]. Limitations and applicable ranges of these reshock models are summarized in Table 1.

Charakhch'an's model and Mikaelian's reshock model agree with the assumption that the reshock growth rate is not a function of either k or h_r. In fact, past experiments have indicated that the growth rate after a reshock is independent of the interface shape [28,29,37] for 3D multi-mode RMI. Vetter and Sturtevant [28] performed RMI with reshock and found that the post-reshock growth rates follow the Mikaelian's reshock model. Later, Erez et al. [37] showed that the initial membrane thickness does not influence the post-reshock growth rate, although it affects the growth rate after the incident shock. More recently, Leinov et al. [29] performed experiments of RMI with reshock for different wall distances and reshock Mach numbers, and found that the reshock growth follows the Mikaelian's reshock models with slightly larger coefficients, i.e., $C \approx 0.38$. These experimental results clearly indicate that the post-reshock growth rate is not a function of the interface condition at reshock. However, Charakhch'an's and Mikaelian's reshock models are only appropriate for a specific regime of RMI and cannot be applied to the same RMI configuration. For example, if dh_1/dt is very small, Charakhch'an's model and Mikaelian's reshock model have the same equation with different values of the coefficient. Charakhch'an's model with $\beta = 1.25$ predicts $\mathrm{d}h_2/\mathrm{d}t$ more than four times as large as that with Mikaelian's reshock model ($C = 0.28$). This significant difference is caused by the mixing conditions at the interface. For instance, experiments usually disturb the interface which results in a relatively thick mixing zone; however, Charakhch'an performed numerical analysis with Lagrangian tracking of the interface due to which the interface stays sharp and simple. Thus, Charakhch'an's model does not consider the diffusion layer and turbulent mixing which can be a prominent physical phenomenon in the experiments. Furthermore, since there is serious scarcity of data about the single-mode RMI after reshock, Charakhch'an's model is not yet fully validated. Therefore, re-investigation of the coefficient is performed in the present work.

Since most of the experimental studies are performed in shock tubes with a flat membrane separating two gases [28,29,38,39], it is hard to obtain the exact initial perturbation shapes for numerical simulation. This is a serious issue since the initial interface shape can be very critical for RMI because the vorticity is deposited only when a shock hits the interface. Past numerical attempts approximated the initial conditions from a configuration of a wire mesh used to support a membrane. For instance, numerical studies undertaken by [40–43] used an egg-carton type perturbation to model the RMI experiments with the membrane supported by a cross wired mesh [28]. Moreover, Schilling and Latini

Table 1 List of existing reshock models

	Interface geometry	Function	Limitation
Mikaelian's potential model [32]	2D single-mode	$h_\mathrm{r}, k, \Delta V_2$	$h_\mathrm{r} \ll k$
Brouillette and Sturtevant model [33]	2D single-mode	$h_\mathrm{r}, k, \Delta V_2$	$h_\mathrm{r} \ll k$
Charakhch'an's model [34]	2D single-mode	ΔV_2	
Mikaelian's reshock model [35]	3D multi-mode	ΔV_2	

[42] investigated the effect of the magnitude of the random noise on the late time growth rates and also compared it with Mikaelian's model. Mügler and Gauthier [44] performed a 2D numerical study of the experiments by Poggi et al. [39], with initial conditions defined as a combination of sinusoidal waves with eight different wavelengths that are in the same order of the wire mesh spacing. Although these wire-based initializations provide a good approximation for the wavelength, the estimation of the initial amplitude is still ambiguous because it is difficult to precisely measure how much the membrane is pushed into the wire mesh before it ruptures. Therefore, Leinov et al. [29] neglected the wire mesh supports, and simply modeled the initial perturbation as a summation of sinusoidal planes with different wavelengths and amplitudes.

Apart from the flat membrane settings, Schilling et al. [45] briefly analyzed the post-reshock growth rates of 2D single-mode RMI based on the membrane-less experiment performed by Collins and Jacobs [11]. These numerical studies have tested a limited type of initial perturbation shape, and the effect of initial conditions is not fully understood yet. Given these observations, it is clear that there still remains some uncertainty about RMI growth after reshock. Therefore, the present work investigates reshocked RMI for four different combinations of initial interface geometry and perturbation: 2D single-mode, 3D single-mode, 2D multi-mode and 3D multi-mode, and investigates the differences in the ensuing growth rates. Since the experimental validations of the post-reshock growth rates are only available for 3D multi-mode RMI, the latest reshocked RMI experiments by Leinov et al. [29] are chosen as a base configuration, and the other types of perturbation shapes are examined under the same conditions. Then, parametric studies of each type of initial interface shapes are performed to investigate the controlling factor of the reshocked RMI growth rates.

This paper is organized as follows. The governing equations, numerical schemes and initial conditions are presented in Sect. 2. The simulation results of the experimental setup are presented in Sect. 3.1 and the parametric studies of single- and multi-mode RMI are discussed in Sects. 3.2 and 3.3, respectively. Finally, the conclusions are reported in Sect. 4.

2 Simulation methodology

The unsteady, compressible Navier–Stokes equations for multi-species flows are:

$$\frac{\partial \rho}{\partial t} + \frac{\partial \rho u_i}{\partial x_i} = 0, \tag{6}$$

$$\frac{\partial \rho u_i}{\partial t} + \frac{\partial}{\partial x_j}\left[\rho u_i u_j + P\delta_{ij} - \tau_{ij}\right] = 0, \tag{7}$$

$$\frac{\partial \rho E}{\partial t} + \frac{\partial}{\partial x_i}\left[(\rho E + P)u_i + q_i - u_j \tau_{ij}\right] = 0, \tag{8}$$

$$\frac{\partial \rho Y_k}{\partial t} + \frac{\partial}{\partial x_i}\left[\rho Y_k u_i + J_{i,k}\right] = 0 \quad k = 1, \ldots, N_s, \tag{9}$$

for the continuity, momentum, energy and species equations, respectively. Here, ρ is the density, $(u_i)_{i=1,2,3}$ is the velocity vector in Cartesian coordinates, P is the pressure, E is the total energy, Y_k is the mass fraction for species k, τ_{ij} is the shear stress tensor, q_i is the rate of heat transfer, $J_{i,k}$ is the species diffusion flux, and N_s is the total number of species in the flow.

The total energy, E is defined as:

$$E = e + \frac{1}{2}u_k u_k, \tag{10}$$

where e is the internal energy given as:

$$e = \sum_{k=1}^{N_\mathrm{s}} Y_k h_k - \frac{P}{\rho}, \tag{11}$$

and the sensible enthalpy of k-th species, h_k is obtained as:

$$h_k(T) = \Delta h^0_{f,k} + \int_{T_0}^{T} c_{P,k}(T')\,\mathrm{d}T', \tag{12}$$

where T is the temperature, T_0 is the reference temperature, $\Delta h^0_{f,k}$ is the enthalpy of formation at the reference temperature and pressure, and $c_{P,k}$ is the specific heat at constant pressure.

Thermodynamic variables are computed assuming a calorically perfect gas, which is consistent with previous studies of RMI [41]. Thus, the equation of state can be represented as

$$P = \rho R T, \tag{13}$$

where R is the gas constant, computed as:

$$R = \sum_{k=1}^{N_\mathrm{s}} Y_k \frac{R_\mathrm{u}}{\mathrm{MW_k}}, \tag{14}$$

where R_u is the universal gas constant and $\mathrm{MW_k}$ is the molecular weight of the kth species.

Assuming the fluid to behave Newtonian, the shear stress tensor, τ_{ij} is proportional to the rate of strain defined as:

$$\tau_{ij} = \mu\left(\frac{\partial u_i}{\partial x_j} - \frac{\partial u_j}{\partial x_i}\right) - \frac{2}{3}\delta_{ij}\mu\frac{\partial u_k}{\partial x_k}, \tag{15}$$

where μ is the molecular viscosity coefficient. The molecular viscosity coefficient in the mixture of multiple fluids is given by the Wilke's formula [46,47]. The rate of heat transfer is computed by Fourier's law assuming that the rate of heat conduction is proportional to the local temperature gradient; in addition, the enthalpy changes caused due to species diffusion must be considered as well. Thus, the heat flux is given as:

$$q_i = -\kappa \frac{\partial T}{\partial x_i} + \rho \sum_{i=1}^{N_s} Y_k h_k V_{i,k}. \tag{16}$$

There are various models to compute the diffusion velocities. The present study uses the mixture averaged formulation [48] given as:

$$V_{i,k} = -\frac{1}{X_k} D_{km} \frac{\partial X_k}{\partial x_i}, \tag{17}$$

where $V_{i,k}$ is the diffusion velocity, X_k is the mole fraction of the kth species and D_{km} is the mixture diffusion coefficient for the kth species. The diffusion flux of the kth species is given as:

$$J_{i,k} = \rho Y_k (V_{ik} + V_i^c), \tag{18}$$

where

$$V_i^c = -\sum_{k=1}^{N_s} Y_k \left(\frac{1}{X_k} D_{km} \frac{\partial X_k}{\partial x_i} \right). \tag{19}$$

A challenge for the RMI simulation is to capture the large gradients as well as to accurately resolve the smooth regions encountered in the flow field. Past studies [49,50] have proposed hybrid algorithms that involve a shock capturing scheme to compute the flow in regions of sharp discontinuities, and a central-type scheme for smoother regions of the flow. For example, Fryxell and Menon [51] demonstrated a similar hybrid scheme that uses a fourth order scheme in smooth regions of the flow and the Piecewise-Parabolic method (PPM) in the regions dominated by discontinuities, and applied it to study RMI. Hill et al. [41] used another type of a hybrid scheme with tuned-center difference (TCD) in the smooth regions and Weighted Essentially Non-Oscillatory (WENO) for shock capturing, and applied it to study RMI. Here, we follow a similar approach which uses a higher-order scheme to resolve smooth regions as well as discontinuities at the same time. The numerical scheme uses a fourth-order central scheme, well adapted to turbulent simulations in smooth regions. The flux evaluation, however, reverts to a fourth-order flux difference splitting method in regions of strong gradients. The Monotone Upstream-centered Schemes for Conservation Laws (MUSCL) approach is used to reconstruct the flux at discontinuities, and a hybrid Riemann solver, HLLC/E, is applied to obtain fluxes [49]. The hybrid scheme has been successfully validated for shock-turbulence interaction [49], turbulent mixing in supersonic flows [50], and it has been successfully applied to 2D RMI [52]. Details are therefore avoided for brevity.

The computational domain in this study is taken from the recent experimental study of reshocked RMI performed by Leinov et al. [29], and is shown in Fig. 3. The streamwise length (L_x) is 16 cm, and the shock and the perturbed interface are located at 9 and 8 cm from the end wall, respectively. An ambient temperature of 298 K and atmospheric pressure

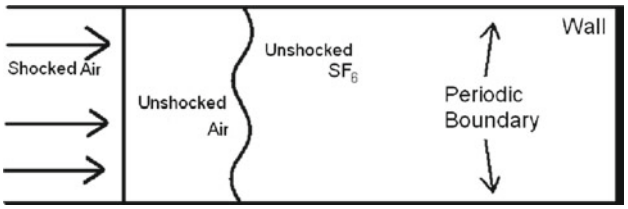

Fig. 3 Schematic of the RMI test configuration. For reshock, the shock reflects from the *right* wall and exits from the *left*

is considered for the initial unshocked region. For 2D, the transverse length is 1 cm, and the simulation domain is discretized with a grid size of $2,048 \times 128$. For 3D, the cross sectional area is 1×1 cm, and the simulation domain is discretized with a $1,024 \times 64^2$ grid. Periodic BC is used in the transverse direction for both 2D and 3D studies. Grid independence of the growth rate is shown in Sect. 3. The incident shock Mach number is 1.2, and SF_6 and air are chosen as the species for the high and low density fluids across the interface. The effects of initial conditions on the post-reshock growth rate have been addressed recently [42,43]. However, these studies focus on a few limited cases and robust parametric studies have not been hitherto performed. This study investigates four types of initial interface shapes such as 2D single-mode, 2D multi-mode, 3D single-mode and 3D multi-mode. The species interface is initialized with a thin diffusion layer using the function introduced by Latini et al. [53] to make the initial conditions less sensitive to the grid geometry. For these initial conditions, the reshock hits the interface at around $t = 0.75$ ms and the expansion wave from the end wall reaches the interface at $t \approx 1.2$ ms. The parametric studies performed in Sects. 3.2 and 3.3 use these initial conditions as the baseline to analyze the effect of the different parameters for appropriate models.

Of preponderant interest in this study is to determine the mixing length growth behavior for different geometries and initial conditions. There are different methods to calculate the mixing length from numerical results. One approach is the threshold method that defines the mixing length as the region where $\epsilon < \langle Y_{\text{air}} \rangle < 1 - \epsilon$, where $\langle Y_{\text{air}} \rangle$ denotes the line (2D) or planer (3D) average mass fraction of air, and ϵ is a small number [24,40]; $\epsilon = 0.01$ is used in this study. The threshold measure is widely used for single and multi-mode studies, but the mixing length is influenced by the value of ϵ. Experimental studies usually utilize the threshold-type method by taking a picture of the interface, but the definition of boundaries are not clearly defined in terms of the mass fraction. The other method is to measure the amplitude of the iso-contour of the mass fraction [33]. This iso-contour definition corresponds to theoretical values, and the diffusion thickness can be ignored, but is practically limited to single-mode studies only since it cannot account for well mixed

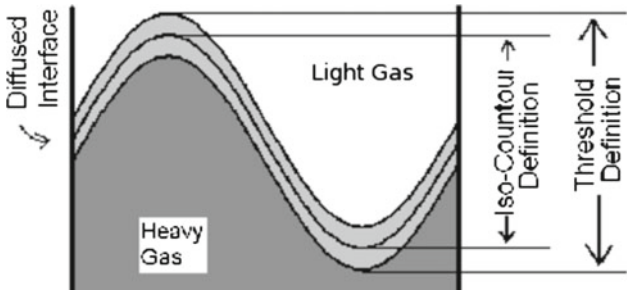

Fig. 4 Differences in the mixing layer estimate by different methods

regions. The difference between the threshold and iso-contour definition is shown in Fig. 4.

3 Results

The growth rate after reshock under various initial interface shapes are analyzed. First, four types of different initial interface shapes are examined based on the experimental setup of Leinov et al. [29] and a recent numerical investigation on the pre-reshock growth of 2D single-mode RMI [52]. Then, parametric studies are performed to find out the important factors that determine the post-reshock growth rates.

3.1 Simulation of experimental setups

Based on the experimental setups of Leinov et al. [29], four initial conditions for RMI, i.e., 2D single-mode, 3D single-mode, 2D multi-mode and 3D multi-mode are simulated and are presented here. The initial conditions for single-mode RMI in 2D and 3D are defined as [11,25]:

$$\begin{aligned} a(y) &= a_0 \sin(\tfrac{2\pi}{\lambda} y) && \text{(2D)};\\ a(y,z) &= a_0 \left[\sin(\tfrac{2\pi}{\lambda} y) + \sin(\tfrac{2\pi}{\lambda} z)\right] && \text{(3D)}. \end{aligned} \tag{20}$$

Similarly, multi-mode perturbation is defined as the superposition of multiple wavelengths (21) used by Leinov et al. [29] and Banerjee and Andrews [54].

$$\begin{aligned} a(y) = \frac{a_0}{\sigma} \sum_{k_y=1}^{k_{\max}} \Bigg[& a_{1,k} \cos\left(\frac{2\pi k_y y}{L_y} + \alpha_{1,k}\right) \\ & + a_{2,k} \sin\left(\frac{2\pi k_y y}{L_y} + \alpha_{2,k}\right)\Bigg] \quad \text{(2D)}; \\ a(y,z) = \frac{a_0}{\sigma} \sum_{k_z=1}^{k_{\max}} \sum_{k_y=1}^{k_{\max}} \Bigg[& a_{1,k} \cos\left(\frac{2\pi k_y y}{L_y} + \alpha_{1,k}\right) \\ & \times \sin\left(\frac{2\pi k_z z}{L_z} + \beta_{1,k}\right) + a_{2,k} \sin\left(\frac{2\pi k_y y}{L_y} + \alpha_{2,k}\right) \\ & \times \sin\left(\frac{2\pi k_z z}{L_z} + \beta_{2,k}\right) + a_{3,k} \sin\left(\frac{2\pi k_y y}{L_y} + \alpha_{3,k}\right) \\ & \times \cos\left(\frac{2\pi k_z z}{L_z} + \beta_{3,k}\right) + a_{4,k} \cos\left(\frac{2\pi k_y y}{L_y} + \alpha_{4,k}\right) \\ & \times \cos\left(\frac{2\pi k_z z}{L_z} + \beta_{4,k}\right)\Bigg] \quad \text{(3D)}. \end{aligned} \tag{21}$$

Table 2 List of parameters used to construct species interface perturbations

	$k_{\max}$	a_0 (mm)	Grid size
Case 2D single-mode		0.5	$2{,}048 \times 128$
Case 2D multi-mode	8	2.0	$2{,}048 \times 128$
Case 3D single-mode		1.0	$1{,}024 \times 64^2$
Case 3D multi-mode	4	2.0	$1{,}024 \times 64^2$

Here, λ is the wavelength, k_y and k_z are the wavenumbers in y- and z-directions with values between 1 and $k_{\max}$, $a_{i,k}$ are random coefficients between -1 and 1, $\alpha_{i,k}$ and $\beta_{i,k}$ are random coefficients between $-\pi$ and π, L_y and L_z are the domain sizes in y- and z-directions, σ is the standard deviation of the summation part to normalize the fluctuation to be one, and the initial amplitude, a_0, determines the size of the perturbation. The parameters used for the simulation are summarized in Table 2.

Grid sensitivity of the growth rate is checked for each of the simulation cases. 2D studies utilize 128 grids in the y-direction, and good agreement with a finer grid ($4{,}096 \times 256$) are seen in both single- and multi-mode RMI as suggested in a previous numerical study [24]. These results are presented in Fig. 5: single-mode in (a) and multi-mode in (b). Similarly, 3D RMI with 64^2 cross-sectional grid shows good agreement with a finer grid ($1{,}546 \times 96^2$). Note that the amplitude growths in 2D and 3D single mode cases become grid dependent after the reflected expansion wave reaches the species interface at $t = 1.2$ ms. Even though the dynamics of large scale motion such as mixing height growth are grid independent, the small scale vortices are still grid dependent, so that the small RMI structures caused by reshock may be enhanced by the reflected expansion wave, and the growth rates become grid dependent as also observed in past works [45,53]. In multi-mode RMI, both coarse and fine grids result in similar growth in all time regimes since the small scale differences are less significant compared to the disturbance caused by the multi-mode interface. However, this study will not discuss the time regimes.

The pre-reshock growth rates of 2D and 3D single-mode RMI are also good measures to check the numerical schemes, since there are reliable theoretical and empirical models widely validated in the literature [11,19,24–26]. Sadot et al. [22] obtained the empirical model for the growth rate as:

$$a_{b/s}(t) = v_0 \frac{1 + v_0 k t}{1 + D v_0 k t + E v_0^2 k^2 t^2}. \tag{22}$$

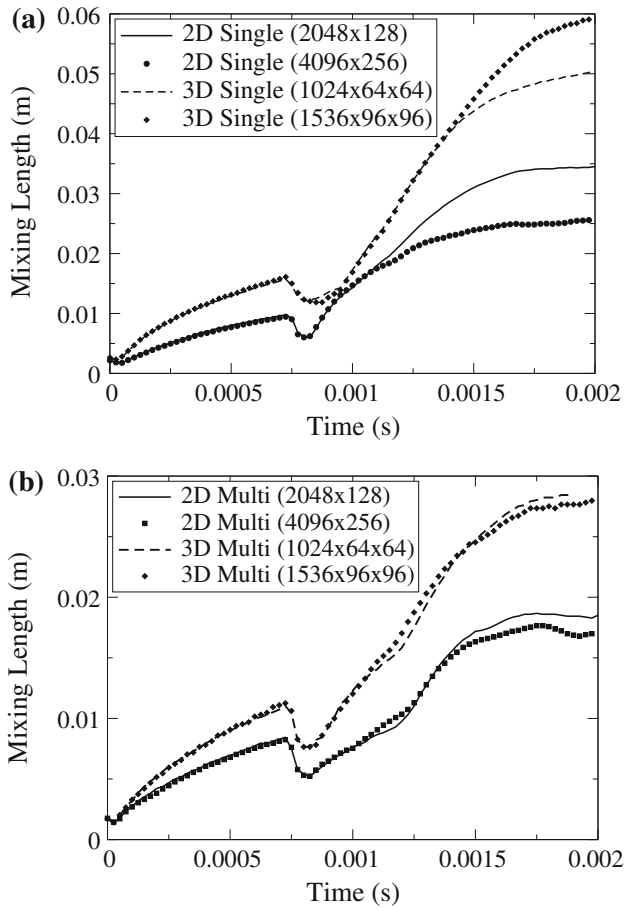

Fig. 5 Grid sensitivity of single- and multi-mode RMI in 2D and 3D

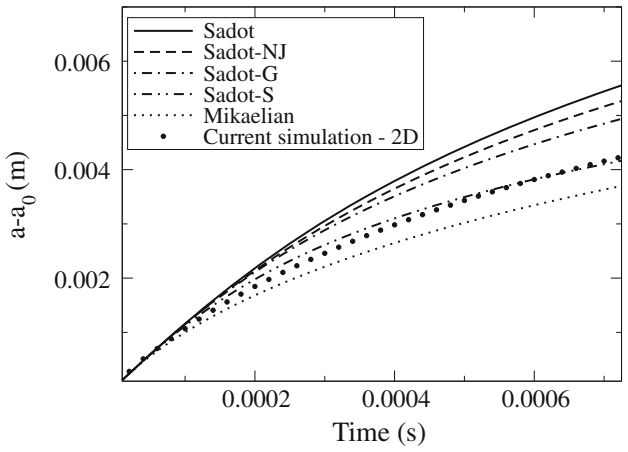

Fig. 6 Comparison with the 2D RMI growth rate models

The coefficients D and E can be chosen based on different theories and are summarized in Table 3. Note that the $\pm$ in Table 3 denotes the value used for the bubbles and spikes, respectively.

The theoretical explicit time-dependent expression obtained by Mikaelian [21] is:

$$ka_{b/s}(t) = \begin{cases} kv_0t & \text{if } kv_0t \le a^*; \\ a^* + \frac{C}{1\pm A}\ln\left[1 + \frac{1\pm A}{C}(kv_0t - ka^*)\right] & \text{if } kv_0t > a^*, \end{cases} \quad (23)$$

where $C = (3 \pm A)/3$ for 2D and $C = 2$ for 3D; a^* is the amplitude to reach non-linear growth rates, chosen as $a^* = \frac{1}{2k}$ for 2D and $a^* = \frac{1}{3k}$ for 3D. The comparisons between models and numerical simulations are shown in Figs. 6 and 7 for 2D and 3D, respectively. Note that the iso-contour definition is used to exclude diffusion thickness to be precisely comparable to models. The numerical result closely follows Sadot-Sohn model for 2D and Mikaelian for 3D, and this test exemplifies that the numerical predictions are in accordance with the theoretical models. Note that the validation study of multi-mode RMI has not performed in this study since the growth models highly depends on the statistical approach and not yet as established as the single-mode models.

The comparisons of growth rates for each of the simulation cases are shown in Fig. 8 and are summarized in Table 4. Each study shows distinctly different growth rates after reshock. 3D multi-mode RMI predicts the growth rate very close to the experimental value. However, 2D multi-mode RMI results very small growth rates compared to the 3D multi-mode RMI, as also observed by Gowardhan et al. [43]. The single-mode cases tend to have larger growth rates in 2D and 3D. From these results, single-mode and 3D tends to have larger growth rates than multi-mode and 2D. However, there are not enough data sets to argue the reasons for such differences. Therefore, parametric studies in each type of perturbations are performed in the following sub-sections

Table 3 List of coefficients for Sadot-type models

Model	Dimension	D	E
Sadot [22] (Original model)	2D	$1 \pm A$	$[3(1 \pm A)/2(1 + A)]$
Niederhaus and Jacobs [23] (NJ)	2D	$1 \pm A$	$1 \pm A$
Goncharov [20] (G)	2D	$1 \pm A$	$[3(1 \pm A)/(3 + A)]$
Sohn [55] (S)	2D	$1 \pm A$	$(2 \pm A)/2$
Chapman and Jacobs [25] (CJ)	3D	$1 \mp (0.01221A^3 + 0.69844A)$	$(1 \pm A)/2$

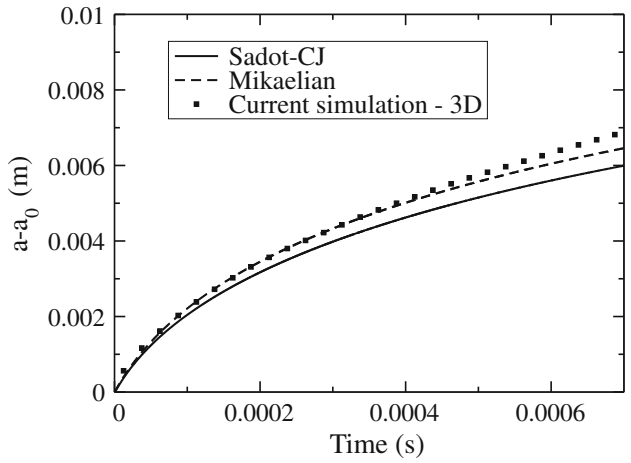

Fig. 7 Comparison with the 3D RMI growth rate models

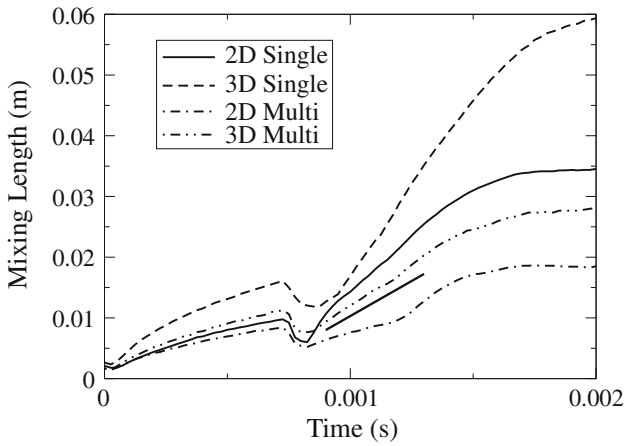

Fig. 8 Comparisons of growth for each of the cases. The *straight-line* represents the experimental slope of 23.1 m/s [29]

Table 4 Growth rates before and after reshock, and model coefficients for each case

	$\frac{dh_1}{dt}$	$\frac{dh_2}{dt}$	C	β
Case 2D single-mode	7.85	34.11	0.52	0.64
Case 3D single-mode	12.50	59.1	0.90	1.09
Case 2D multi-mode		11.65	0.17	
Case 3D multi-mode		25.2	0.38	

C and β are coefficients found from the formulations of Mikaelian's reshock model (5) and Charakhch'an's model (4), respectively, where $\Delta V_2 = 92.5$ m/s and $A^+ = 0.71$

to determine the driving factor of the post-reshock growth rates.

3.2 Parametric studies of single-mode RMI

Even though past studies have reported that the conditions at reshock are likely to be independent of interface conditions, the previous section shows that the interface condition changes the post-reshock growth rates. Therefore, parametric studies are performed to investigate the effect of initial perturbation shapes on the post-reshock growth rates. Here, we first conduct parametric studies in 2D to evaluate the sensitivity of RMI growth rates after reshock to the interface shapes at reshock (h_r and λ) and the incident Mach number, M_1 in both 2D and 3D. The descriptions of each test case considered in this investigation are summarized in Table 5.

First, various initial geometries are tested (Case S1–S5) and are compared to analyze the effect of the interface geometry parameters such as h_r, λ and h_r/λ. Figure 9 predicts that all cases result in similar growth rates (i.e., the slope after reshock). Note that the number of the grid points per perturbation is kept 128 in the y-direction for all these cases. Table 6 summarizes the growth rates and coefficients obtained from the Mikaelian's reshock formulation and Charakhch'an's models, and the values of these coefficients are relatively close, even though λ and h_r are different for each of the cases. Thus, the results suggest that the post-reshock growth rate is not a strong function of wavelength as Charakhch'an suggested [34,56]. Note that Mikaelian's potential model [35] and Brouillette and Sturtevant's model [33] are inappropriate for predicting the growth rate for perturbation amplitudes as large as the ones considered in the current investigation.

The empirical reshock models show that the growth rate is independent of the interface shape at reshock, but ΔV_2 is predicted to be linearly correlated to the growth rates. The post-reshock growth rate with different ΔV_2 in 2D (Case S3, S9–11) and 3D (Case 3DS1–4) are measured by changing the incident Mach number, and the results of post-reshock growth rates are summarized in Table 7. The numerical results show higher growth rates for the cases with the higher incident Mach number, presented in Fig. 10. The linear correlation between the post-reshock growth rate and ΔV_2 in both 2D and 3D are found, as previously reported in the 3D RMI experiment with random perturbations [29], and is presented in Fig. 11 for 2D.

Comparisons to empirical models are performed. Using the formulation of Charakhch'an's model, which is appropriate for 2D single-mode RMI, the coefficient $\beta \approx 0.68$ with the range of $0.59 < \beta < 0.84$ is obtained in the current simulations, but the original value proposed by Charakhch'an is about twice as large, $\beta \approx 1.25$, that is obtained from the average of multiple numerical experiments with the range of $0.53 < \beta < 1.50$ [34]. Thus, the results from the current study are within the range of Charakhch'an's studies, even though average values are underestimated. The difference could be due to the diffusion layer which is not considered in Charakhch'an's numerical simulations. However, it is clear that Mikaelian's potential model over-predicts the growth rate by comparing β and $\frac{2\pi h_r}{\lambda}$. Assuming a correlation similar to Mikaelian reshock model, the numerical study reveals

Table 5 Cases simulated for 2D and 3D single-mode RMI

	Dimension	Total grid	Domain size (cm)	a_0 (mm)	L (mm)	λ (mm)	M_1
Case S1	2D	2,048 × 128	16.0 × 1.0	0.5	40	10.0	1.2
Case S2	2D	2,048 × 128	16.0 × 1.0	0.5	80	10.0	1.2
Case S3	2D	8,192 × 128	16.0 × 0.25	0.125	20	2.5	1.2
Case S4	2D	4,096 × 128	16.0 × 0.5	0.25	40	5.0	1.2
Case S5	2D	1,024 × 128	16.0 × 2.0	1.0	80	20.0	1.2
Case S6	2D	2,048 × 128	16.0 × 1.0	0.5	80	10.0	1.1
Case S7	2D	2,048 × 128	16.0 × 1.0	0.5	80	10.0	1.3
Case S8	2D	2,048 × 128	16.0 × 1.0	0.5	80	10.0	1.4
Case 3DS1	3D	1,024 × 64^2	16.0 × 1.0^2	1.0	80	10.0	1.1
Case 3DS2	3D	1,024 × 64^2	16.0 × 1.0^2	1.0	80	10.0	1.2
Case 3DS3	3D	1,024 × 64^2	16.0 × 1.0^2	1.0	80	10.0	1.3
Case 3DS4	3D	1,024 × 64^2	16.0 × 1.0^2	1.0	80	10.0	1.4

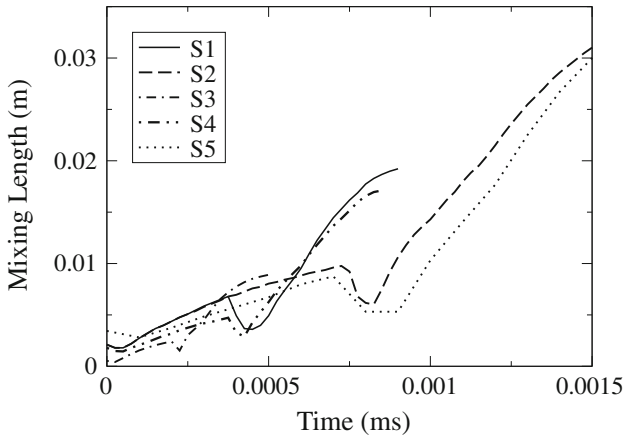

Fig. 9 Mixing length growth with different initial geometries

Table 6 2D single-mode RMI for different h_r and λ

Case	S1	S2	S3	S4	S5
$\frac{dh_1}{dt}$	12.50	7.85	7.42	7.81	10.15
$\frac{dh_2}{dt}$	42.50	34.11	33.83	39.84	40.15
h_r (mm)	6.48	9.77	2.42	4.72	8.75
λ (mm)	10.0	10.0	2.5	5.0	20.0
$\frac{2\pi h_r}{\lambda}$	4.07	6.13	6.08	5.93	2.75
β	0.84	0.64	0.63	0.73	0.77
C	0.65	0.52	0.52	0.61	0.61

$C \approx 0.56$ for 2D and $C \approx 0.84$ for 3D, that are larger than the originally proposed value. There is no experimental data available for the validation yet. Schilling et al. [45] performed the numerical analysis of 2D single-mode RMI with reshock and found similar correlations, $C \approx 0.56$ (however, the value of the slope identified in the title of their Fig. 9 [45] differs from the actual slope in their figure by a factor of two). Thus, both empirical models can be applied to the reshock models with proper coefficients.

Table 7 2D and 3D single-mode RMI with different incident Mach numbers

Case	S6	S2	S7	S8	3DS1	3DS2	3DS3	3DS4
M_1	1.1	1.2	1.3	1.4	1.1	1.2	1.3	1.4
ΔV_1	45.9	68.5	99.2	127.5	45.9	68.5	99.2	127.5
ΔV_2	57.4	92.5	133.7	173.5	57.4	92.5	133.7	173.5
$\frac{dh_1}{dt}$	5.00	7.85	9.06	10.30	9.38	12.50	14.28	18.12
$\frac{dh_2}{dt}$	20.08	34.11	51.92	68.89	34.73	59.09	89.06	94.36
A^+	0.70	0.71	0.74	0.78	0.70	0.71	0.74	0.78
β	0.62	0.63	0.62	0.59	1.10	1.09	1.04	0.83
C	0.50	0.51	0.52	0.51	0.86	0.90	0.90	0.70

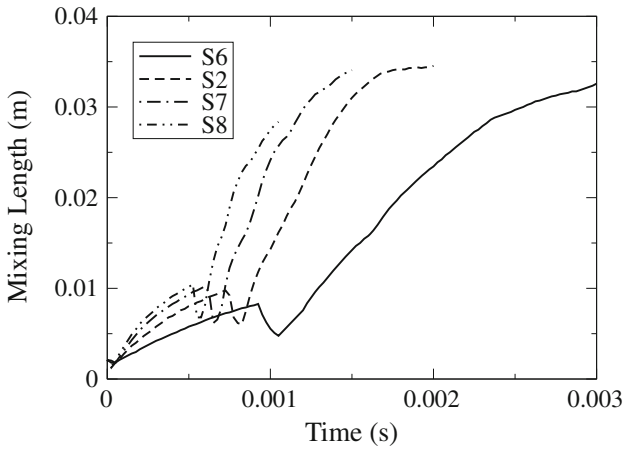

Fig. 10 Amplitude of 2D RMI with different incident Mach numbers

The differences in the evolution of 2D (Case S2) and 3D (Case 3DS2) are presented in Figs. 12 and 13. At 0.7 ms, the species interface creates the typical mushroom shape of the interface. The 3D case shows roll-ups for both bubble and spike fronts, instead of both bubbles and spikes sharing the same roll-up as in 2D. The difference is because that 2D RMI generates vortex lines, whereas 3D RMI create vortex rings around both bubbles and spikes. When the reshock hits the perturbation, the interface is distorted (0.8 ms), and the inversion of bubble and spike occurs as seen in Fig. 2 (0.9 ms) and show rapid growth at later times. Similar RMI evolution has been reported in past studies as well [11,19,24–26,45].

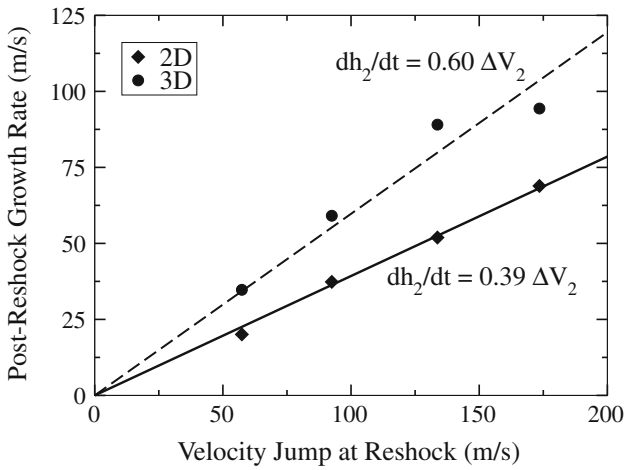

Fig. 11 Correlation between mixing length growth rate and ΔV_2. The regression line shows that the slope is 0.39 in 2D and 0.60 in 3D

Even though the shape of RMI perturbation at reshock does not influence the post-reshock growth rate, the dimensionality of perturbation is an important factor as often discussed in classical reshock models [25,57]. 3D single-mode results show $C \approx 0.84$ and $\beta \approx 1.02$, which are about 1.6 times larger than the values obtained from the 2D single-mode studies ($C \approx 0.52$ and $\beta \approx 0.63$). Although the differences in the post-reshock growth in 2D and 3D have not been analytically obtained, a couple of possible reasons are briefly discussed here. First, the vortex stretching term in (1) is activated in 3D flow, whereas this term is zero in 2D; this vortex stretching term can possibly strengthen the vorticity if the vortex rings are stretched. The other possible reason is due to the geometry of the perturbation. The 3D RMI will have a point contact to the shock at the bubble and spike fronts, whereas 2D RMI will have a line contact to the shock. Thus, it is possible for 3D RMI to have larger vorticities at fronts that can cause larger growth rates.

In summary, the parametric study of single-mode RMI shows that the post-reshock growth rate is independent of the wavelength and mixing length at reshock, and linearly correlated with ΔV_2. However, the dimension of the perturbation

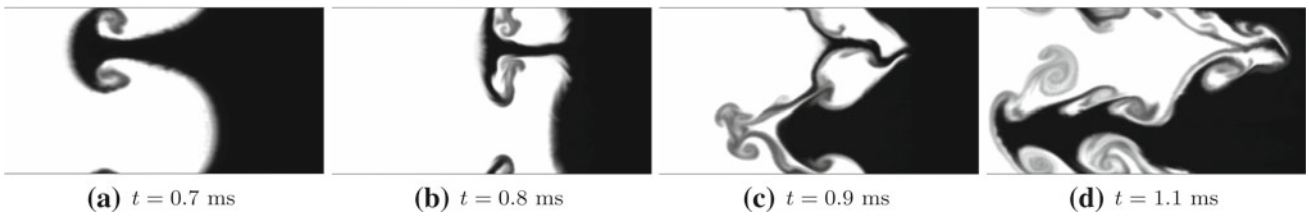

Fig. 12 RMI interface shape colored by mass fraction of SF_6 (Case S2)

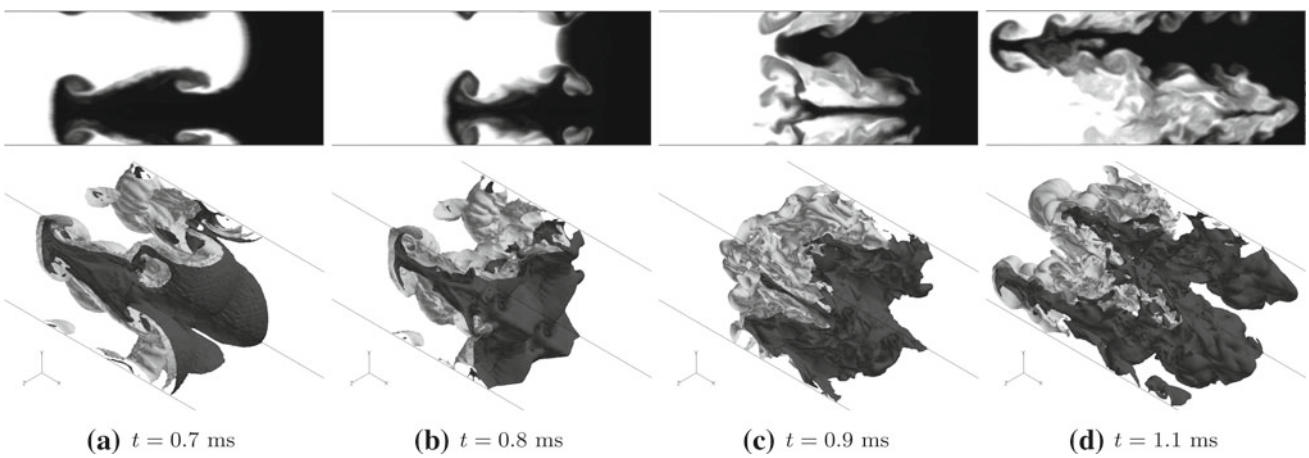

Fig. 13 *Top* RMI interface shapes colored by mass fraction of SF_6, *Bottom* iso-surfaces of species interface with different mass fractions of SF_6 (*Light* 10%, *Dark* 90%)

Table 8 List of initial conditions and results for the 2D and 3D multi-mode RMI

	Dimension	$k_{\max}$	a_0 (mm)	R	Grid size	$\frac{dh_2}{dt}$	C
Case M1	2D	2	2.0	0.4	$2,048 \times 128$	35.60	0.53
Case M2	2D	4	2.0	0.8	$2,048 \times 128$	11.98	0.18
Case M3	2D	8	2.0	1.6	$2,048 \times 128$	11.65	0.17
Case M4	2D	4	0.5	0.2	$2,048 \times 128$	32.50	0.49
Case M5	2D	4	1.0	0.4	$2,048 \times 128$	20.62	0.31
Case M6	2D	4	4.0	0.8	$2,048 \times 128$	13.28	0.20
Case M7	2D	4	8.0	1.6	$2,048 \times 128$	15.82	0.23
Case 3DM1	3D	2	1.0	0.1	$1,024 \times 64^2$	61.2	0.93
Case 3DM2	3D	2	2.0	0.2	$1,024 \times 64^2$	54.5	0.83
Case 3DM3	3D	2	4.0	0.4	$1,024 \times 64^2$	20.2	0.31
Case 3DM4	3D	2	8.0	0.8	$1,024 \times 64^2$	23.6	0.36
Case 3DM5	3D	4	1.0	0.2	$1,024 \times 64^2$	53.1	0.81
Case 3DM6	3D	4	2.0	0.4	$1,024 \times 64^2$	25.2	0.38
Case 3DM7	3D	4	4.0	0.8	$1,024 \times 64^2$	26.9	0.41
Case 3DM8	3D	4	8.0	1.6	$1,024 \times 64^2$	27.5	0.42

is important and 3D cases result in 1.6 times larger growth rates than counterpart 2D cases.

3.3 Parametric studies of multi-mode RMI

Since single-mode RMI studies show that the growth rate is not a strong function of the interface geometry, the same reshock growth model should ideally be applicable to multi-mode RMI. In fact, Charakhch'an [34,56] analyzed the post-reshock growth rates of the interface which consists of three segments of lines instead of a sinusoidal wave, and demonstrated that his model was applicable to the case. However, the post-reshock growth rates of multi-mode RMI are smaller than single-mode cases in 2D and 3D, as shown in Sect. 3.1. Therefore, the growth rate is expected to depend also on the randomness of the initial perturbation. Here, we investigate the growth rate of multi-mode RMI in 2D and 3D with different initial amplitudes and wavenumbers. The $\frac{dh_2}{dt}$ and C obtained for each case are presented in Table 8.

Analyzing the results, the post-reshock growth rates of multi-mode RMI show two different sets of solution based on the initial interface shapes. The first type of the solution is "rapid growth", which is the post-reshock growth rate close to the single-mode RMI. For 2D multi-mode RMI study, small $k_{\max}$ and amplitude cases such as Case M1 and M4 show that the large post-reshock growth rate ($C \approx 0.52$) is comparable to the single-mode 2D RMI ($C \approx 0.56$). Similarly, the 3D cases show rapid growth with small amplitudes and wavenumbers (Case 3DM1, 3DM2 and 3DM5) with growth rate constant, $0.81 < C < 0.93$, comparable to the single-mode solution ($C \approx 0.90$). On the other hand, "slow growth" is seen when the initial interface shape is more random (lager a_0 and $k_{\max}$). 2D cases result in $C \approx 0.2$ as seen in Cases M2, M3, M6 and M7, and 3D RMI cases show $0.31 < C < 0.42$. Thus, the slow-growth cases seem to have a value of C only about 40% of the rapid-growth in both 2D and 3D studies, presented in Fig. 14. Thus, assuming a_0 and $k_{\max}$ to be the only parameters that determine whether the mixing layer growth rate is rapid or slow, we define the Randomness factor as

$$R = \frac{a_0 k_{\max}}{L_y} \tag{24}$$

to quantify the initial perturbation. Note that L_y is used to normalize the parameter. When R is small, the growth rates follow single-mode cases. In this study, for example, rapid-growth is likely to happen when $R \leq 0.4$ for 2D and $R \leq 0.2$ for 3D. The same sets of random parameters are used for each $k_{\max}$ studies (e.g. Case M2, M4, M5, M6 and M7) to focus on the analysis of the initial amplitude. Even though the different random numbers are not explicitly studied within the same test case, the different $k_{\max}$ cases use different sets of random numbers and the effects of R are consistent with different $k_{\max}$ values. Thus, the sensitivities of the choice of random number are expected to be very small.

A fundamental question is to quantify the differences between rapid and slow growths. Past experiments [29] obtained the range of C as $0.33 < C < 0.44$ that agrees well with slow growth data sets ($0.31 < C < 0.42$) obtained from the numerical prediction. 2D simulations also show slower reshock growth rates in multi-mode, as also reported in a recent numerical study [43].

The time series of RMI evolution of rapid growth (Case M4) and slow growth (Case M2) are shown in Fig. 15. Since Case M4 has very small amplitude to begin with, the interface shape is still resolved at reshock, whereas the Case M2 shows a well mixed interface. Thus, bubbles and spikes after reshock happen to grow as fast as the single-mode case, similar to the predictions of Charakhch'an [34,56]. However, Case M2 shows complex mixing at the time of reshock, and bubbles and spikes carry lateral motion that cease the growth of the mixing length in the longitudinal direction but enhances the mixing of species. Similar behaviors of bubbles and spikes are seen in 3D as well, and are presented in Fig. 16. Thus, even though past experimental studies [28,29,37] have shown that the interface conditions do not influence the reshock, the randomness of the interface can play a significant role in the post-reshock growth rates. When an experiment is performed with a flat-membrane, the real interface is inevitably random, and so the randomness criterion is usually satisfied.

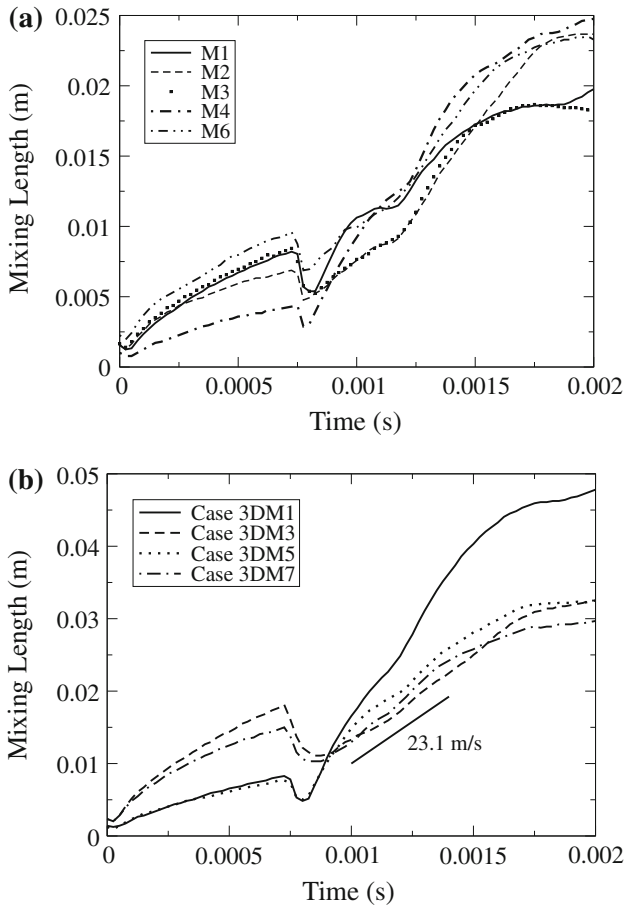

Fig. 14 Mixing length growth of 2D (**a**) and 3D (**b**) multi-mode RMI with different initial conditions

The main reason for the differences in the growth rates between single- and multi-mode RMI is found to be the nature of the randomness of RMI. If a random interface is present at the time of reshock, the growth rate becomes very small due to the tangential motion of bubbles and spikes. However, if there is no interface mixing caused by interactions of bubbles and spikes, and if the interface shape remains well resolved and sharp (small R), reshock induces the growth rates in the same order of the single-mode RMI. Otherwise, the interaction of contiguous bubbles and spikes complicates the mixing phenomena, with larger bubbles ensuing due to a bubble competition process. Such phenomena play a critical role in the mixing characteristics for milti-mode RMI. This study identifies the randomness factor, R, as a useful means to quantify mixing for multi-mode RMI, both pre- as well as post-reshock.

4 Conclusions

In this paper, the reshocked Richtmyer–Meshkov instabilities for four different classes of interface shapes are numerically studied. The initial domain configurations follow past shock

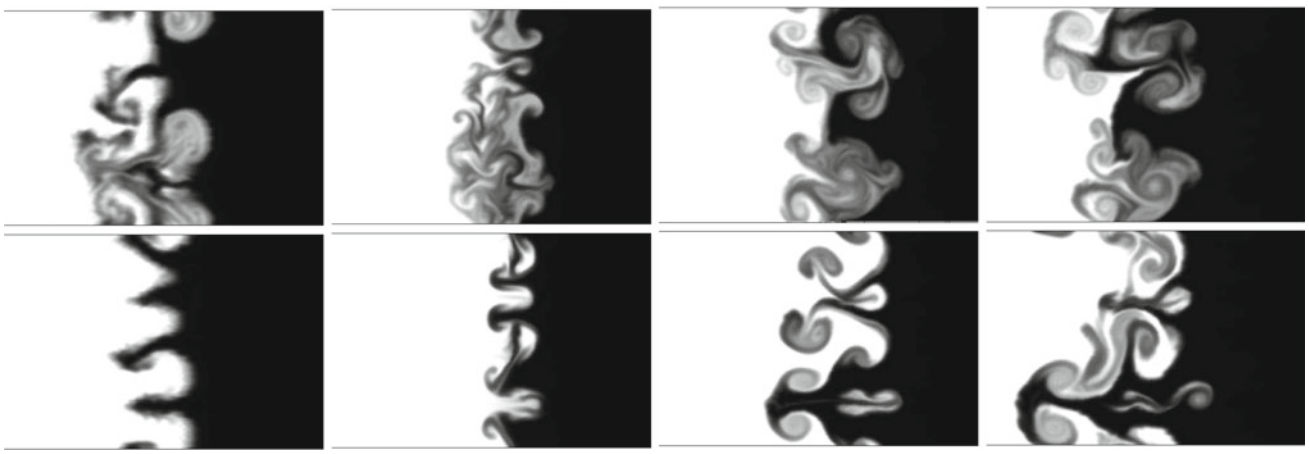

Fig. 15 Side view of interface evolution. *Top* Case M2, *bottom* Case M4. From *left* to *right*, 0.7, 0.8, 0.9 and 1.0 ms

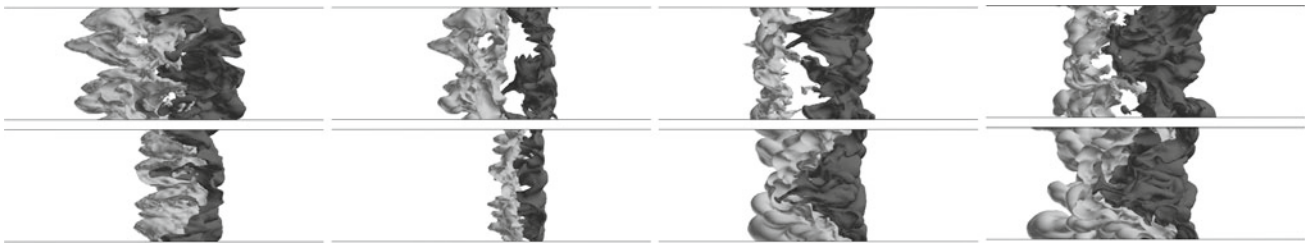

Fig. 16 Side view of interface with different mass fraction of SF_6 (*light* 10%, *dark* 90%). *Top* Case 3DM7, *bottom* Case 3DM5. From *left* to *right*, 0.7, 0.8, 0.9 and 1.0 ms

Table 9 The empirical values for the Mikaelian's reshock model (C) extended for different interface configurations

	2D	3D
Single-mode and multi-mode (sharp interface)	0.55	0.84
Multi-mode (mixed interface)	0.20	0.38

Note that original model use $C = 0.28$, and recent experimental study showed $C = 0.38$ for 3D multi-mode RMI

tube experiments with air/SF_6 species combinations, and the growth rates after the reshock are examined. The parametric studies of 2D/3D single-/multi-mode RMI are performed to investigate the effect of the initial conditions on the late time growth patterns. Single-mode RMI with different wavelengths and wall distances are analyzed to study the sensitivity of interface shapes at reshock, and it is found that growth rates after reshock are a weak function of the interface geometry. Linear correlations of the growth rates to ΔV_2 are found in both 2D and 3D, with higher growth rates for 3D. The value of the coefficient for Charakhch'an's formulation found in this study is about a half of the originally proposed value, but within the range of his numerical experiments. Finally, parametric studies of multi-mode interfaces are performed. The post-reshock growth rates are in the same order as the single-mode RMI (so called "rapid growth") when the interface is not very random. As the initial amplitude and $k_{\max}$ increase, "slow growth" is observed. Furthermore, 3D RMI results in larger growth rates than 2D in multi-mode study as well, and are in agreement with previous experimental data [29]. Key results of the post-reshock growth rate studies can be summarized as:

- The post-reshock growth rates of single-mode RMI in 2D and 3D are not a function of the perturbation geometry parameters such as h_r, λ and $2\pi h_r/\lambda$
- The post-reshock growth rates are linearly proportional to ΔV_2
- The post-reshock growth rates of multi-mode RMI shows rapid-growth if the interface remains sharp at reshock, and slow growth is observed if interface is mixed
- Reshock growth rate in 3D is about 1.6–1.9 times larger than 2D in both single- and multi-mode RMI.

This study suggests that the growth rates of each RMI configuration can be simply characterized by the Mikaelian's reshock model (5) with different values of coefficient obtained by parametric study shown in Table 9.

Acknowledgments This work is supported in part by the Defense Threat Reduction Agency (Dr. S. Peiris, Program Manager) and the Air Force Research Laboratory, Eglin Air Force Base, FL (Dr. D.V. Nance, Program Manager). The computational resources were provided by the Department of Defense High Performance Computing Centers at ERDC, NAVO and ARL.

References

1. Richtmyer, R.D.: Taylor instability in shock acceleration of compressible fluids. Commun. Pure Appl. Math. **13**, 297–319 (1960)
2. Meshkov, E.E.: Instability of the interface of two gases accelerated by a shock wave. Fluid Dyn. **4**(5), 101–104 (1969)
3. Arnett, D.: The role of mixing in astrophysics. Astrophys. J. Suppl. Series **127**, 213–217 (2000)
4. Oran, E.S., Gamezo, V.N.: Origins of the deflagration-to-detonation transition in gas-phase combustion. Combust. Flame **148**, 4–47 (2007)
5. Lindl, J.D., McCrory, R.L., Campbell, E.M.: Progress toward ignition and burn propagation in inertial confinement fusion. Phys. Today **45**, 32–40 (1992)
6. Yang, J., Kubota, T., Zukoski, E.E.: Applications of shock-induced mixing to supersonic combustion. AIAA J. **31**(5), 854–862 (1993)
7. Zabusky, N.J.: Vortex paradigm for accelerated inhomogeneous flows: visiometrics for the Rayleigh–Taylor and Richtmyer–Meshkov environments. Annu. Rev. Fluid Mech. **31**, 495–536 (1999)
8. Niederhaus, J.H.J., Greenough, J.A., Oakley, J.G., Bonazza, R.: Vorticity evolution in two- and three-dimensional simulations for shockbubble interactions. Physica Scripta T132(014019) (2008)
9. Brouillette, M.: The Richtmyer–Meshkov instability. Annu. Rev. Fluid Mech. **34**, 445–468 (2002)
10. Taylor, G.I.: The instability of liquid surfaces when accelerated in a direction perpendicular to their planes. Proc. Royal Soc. London. Series A, Math. Phys. Sci. **201**, 192–196 (1950)
11. Collins, B.D., Jacobs, J.W.: PLIF flow visualization and measurements of the Richtmyer–Meshkov instability of an air/SF_6 interface. J. Fluid Mech. **464**, 113–136 (2002)
12. Layzer, D.: On the instability of superposed fluids in a gravitational field. Astrophys. J. **122**(1), 1–12 (1955)
13. Hecht, J., Alon, U., Shvarts, D.: Potential flow models of Rayleigh–Taylor and Richtmyer–Meshkov bubble fronts. Phys. Fluids **6**(12), 4019–4030 (1994)
14. Mikaelian, K.O.: Analytic approach to nonlinear Rayleigh–Taylor and Richtmyer–Meshkov instabilities. Phys. Rev. Lett. **80**(3), 508–511 (1998)

15. Zhang, Q.: Analyical solutions of Layzer-type approach to unstable interfacial fluid mixing. Phys. Rev. Lett. **81**(16), 3391–3394 (1998)
16. Zhang, Q., Sohn, S.: Nonlinear theory of unstable fluid mixing driven by shock wave. Phys. Fluids **9**, 1106–1124 (1996)
17. Vandenboomgaerde, M., Gauthier, B., Mùgler, C.: Nonlinear regime of a multimode Richtmyer–Meshkov instability: a simplified perturbation theory. Phys. Fluids **14**(3), 1111–1122 (2002)
18. Matsuoka, C., Nishihara, K., Fukuda, Y.: Nonlinear evolution of an interface in Richtmyer–Meshkov instability. Phys. Rev. E **67**, 036301 (2003)
19. Jacobs, J.W., Krivets, V.V.: Experiments on the late time development of single-mode Richtmyer–Meshkov instability. Phys. Fluids **17**, 034105 (2005)
20. Goncharov, V.N.: Analytical model of nonlinear, single-mode, classical Rayleigh–Taylor instability at arbitrary Atwood number. Phys. Rev. Lett. **88**, 134502 (2002)
21. Mikaelian, K.O.: Explicit expressions for the evolution of single mode Rayleigh–Taylor and Richtmyer–Meshkov instabilities at arbitrary Atwood numbers. Phys. Rev. E **67**, 026319 (2003)
22. Sadot, O., Erez, L., Alon, U., Oron, D., Levin, L.A., Erez, G., Ben-Dor, G., Shvarts, D.: Study of nonlinear evolution of single-mode and two-bubble interaction under Richtmyer–Meshkov instability. Phys. Rev. Lett. **80**(8), 1654–1657 (1998)
23. Niederaus, C.E., Jacobs, J.W.: Experimental study of the Richtmyer–Meshkov instability of incompressible fluids. J. Fluid Mech. **485**, 243–277 (2003)
24. Latini, M., Schilling, O., Don, W.S.: High-resolution simulations and modeling of reshocked single-mode Richtmyer–Meshkov instability: comparison to experimental data and to amplitude growth model predictions. Phys. Fluids **19**, 024104 (2007)
25. Chapman, P.R., Jacobs, J.W.: Experiments on the three-dimensional incompressible Richtmyer–Meshkov instability. Phys. Fluids **18**, 074101 (2006)
26. Long, C.C., Krivets, V.V., Greenough, J.A., Jacobs, J.W.: Shock tube experiments and numerical simulation of the single-mode, three-dimensional Richtmyer–Meshkov instability. Phys. Fluids **21**, 114104 (2009)
27. Andronov, V.A., Bakhrakh, S.M., Meshkov, E.E., Mokhov, V.N., Pevnitskii, V.V., Tolshmyakov, A.I.: Turbulent mixing at contact surface accelerated by shock waves. J. Experimental Theor. Phys. **44**, 424 (1976)
28. Vetter, M., Sturtevant, B.: Experiments on the Richtmyer–Meshkov instability. Shock Waves **4**, 247–252 (1995)
29. Leinov, E., Malamud, G., Elbaz, Y., Levin, L.A., Ben-Dor, G., Shvarts, D., Sadot, O.: Experimental and numerical investigation of the Richtmyer–Meshkov instability under re-shock conditions. J. Fluid Mech. **626**, 449–475 (2009)
30. Balakrishnan, K., Genin, F., Nance, D.V., Menon, S.: Numerical study of blast characteristics from detonation of homogeneous explosives. Shock Waves **20**(2), 147–162 (2010)
31. Balakrishnan, K., Menon, S.: On the role of ambient reactive particles in the mixing and afterburn behind explosive blast waves. Combust. Sci. Technol. **182**(2), 186–214 (2010)
32. Mikaelian, K.O.: Richtmyer–Meshkov instabilities in stratified fluids. Phys. Rev. A **31**(1), 410–419 (1985)
33. Brouillette, M., Sturtevant, B.: Experiments on the Richtmyer–Meshkov instability: single-scale perturbations on a continuous interface. J. Fluid Mech. **263**, 271–292 (1994)
34. Charakhch'an, A.A.: Richtmyer–Meshkov instability of an interface between two media due to passage of two successive shocks. J. Appl. Mech. Tech. Phys. **41**(1), 23–31 (2000)
35. Mikaelian, K.O.: Turbulent mixing generated by Rayleigh–Taylor and Richtmyer–Meshkov instabilities. Physica D **36**(3), 343–347 (1989)
36. Read, K.I.: Experimental investigation of turbulent mixing by Rayleigh–Taylor instability. Physica D **12**, 45–58 (1984)
37. Erez, L., Sadot, O., Oron, D., Erez, G., Levin, L.A., Shvarts, D., Ben-Dor, G.: Study of the membrane effect on turbulent mixing measurements in shock tubes. Shock Waves **10**, 241–251 (2000)
38. Houas, L., Chemouni, I.: Experimental investigation of Richtmyer–Meshkov instability in shock tube. Phys. Fluids **8**(2), 614 (1996)
39. Poggi, F., Thorembey, M.H., Rodriguez, G.: Velocity measurements in turbulent gaseous mixtures induced Richtmyer–Meshkov instability. Phys. Fluids **10**(11), 2698–2700 (1998)
40. Cohen, R.C., Dannevik, W.P., Dimits, A.M., Eliason, D.E., Mirin, A.A., Zhou, Y., Porter, D.H., Woodward, P.R.: Three-dimensional simulation of a Richtmyer–Meshkov instability with a two-scale initial perturbation. Phys. Fluids **14**(10), 3692–3709 (2002)
41. Hill, D.J., Pantano, C., Pullin, D.I.: Large-eddy simulation and multiscale modeling of Richtmyer–Meshkov instability with reshock. J. Fluid Mech. **557**, 29–61 (2006)
42. Schilling, O., Latini, M.: High-order WENO simulations of three-dimensional reshocked Richtmyer–Meshkov instability to late times: Dynamics, depoendence on initial conditions, and comparisons to experimental data. Acta Mathematica Scientia **30B**(2), 595–620 (2010)
43. Gowardhan, A.A., Gristein, F.F., Wachtor, A.J.: Three dimensional simulations of Richtmyer–Meshkov instabilities in shock-tube experiments. AIAA-2010-1075, 48th AIAA Aerospace Sciences Meeting, Orlando, FL (2010)
44. Mügler, C., Gauthier, S.: Two-dimensional Navier–Stokes simulations of gaseous mixtures induced by Richtmyer–Meshkov instability. Phys. Fluids **12**, 1783–1798 (2000)
45. Schilling, O., Latini, M., Don, W. S.: Physics of reshock and mixing in single-mode Richtmyer–Meshkov instability. Phys. Rev. E **76**, 026319 (2007)
46. Poling, B.E., Prausnitz, J.M., O'Connell, J.P.: The Properties of Gases and Liquids. McGraw-Hill, New York (2000)
47. Wilke, C.R.: A viscosity equation for gas mixtures. J. Chem. Phys. **18**(4), 517–519 (1950)
48. Poinsot, T., Veynante, D.: Theoretical and Numerical Combustion. Edwards, USA (2005)
49. Génin, F., Menon, S.: Studies of shock/turbulent shear layer interaction using large-eddy simulation. Comput. Fluids **39**(5), 800–819 (2010)
50. Génin, F., Menon, S.: Simulation of turbulent mixing behind a strut injector in supersonic flow. AIAA J. **48**(3), 526–539 (2010)
51. Fryxell, B., Menon, S.: Simulation of turbulent flows containing strong shocks. Physica Scripta **T132**, 014047 (2008)
52. Ukai, S., Balakrishnan, K., Menon, S.: On Richtmyer–Meshkov instability in dilute gas-particle mixtures. Phys. Fluids **22**, 104103 (2010)
53. Latini, M., Schilling, O., Don, W.S.: Effects of WENO flux reconstruction order and spatial resolution on reshocked two-dimensional Richtmyer–Meshkov instability. J. Comput. Phys. **221**, 805–836 (2007)
54. Banerjee, A., Andrews, M.J.: 3D simulation to investigate initial condition effects on the growth of Rayleigh–Taylor mixing. Int. J. Heat Mass Transf. **52**, 3906–3917 (2009)
55. Sohn, S.: Simple potential-flow model of Rayleigh–Taylor and Richtmyer–Meshkov instabilities for all density ratio. Phys. Rev. E **67**, 026301 (2003)
56. Charakhch'an, A.A.: Reshocking at the non-linear stage of Richtmyer–Meshkov instability. Plasma Phys. Control. Fusion **43**, 1169–1179 (2001)
57. Oron, D., Arazi, L., Kartoon, D., Rikanati, A., Alon, U., Shvarts, D.: Dimensionality dependence of the Rayleigh–Taylor and Richtmyer–Meshkov instability late time scaling laws. Phys. Plasmas **8**(6), 2883–2889 (2001)